

# Analysis of Flame Structure and Interactions Between Chemical Reactions, Species Transport and Heat Release in Laminar Flames

Liang Ji, Kalyanasundaram Seshadri\*

*University of California, San Diego, La Jolla, California 92093-0411, USA*

---

## Abstract

A novel method for analyzing counterflow diffusion flames, inspired by Zurdada's sensitivity approach for neural networks, is proposed to identify critical species influencing the heat release rate. By further analyzing concentration changes, this method reveals complex interactions among critical radicals across different temperature zones. The study investigates the auto-ignition temperature of n-heptane and ethanol mixtures within a counterflow flame configuration under low strain rates. In n-heptane dominant mixtures, the inhibition of low-temperature chemistry (LTC) by additional ethanol impacts the heat release rate in the high-temperature zone through the diffusion of specific radicals such as  $\text{CH}_2\text{O}$ ,  $\text{C}_2\text{H}_4$ ,  $\text{C}_3\text{H}_6$ , and  $\text{H}_2\text{O}_2$ . In ethanol-dominant mixtures, higher ethanol fractions increase the heat release rate, primarily due to ethanol decomposition and its subsequent reactions. This method effectively quantifies and compares the influence of both chemical kinetics and species diffusion effects, providing detailed insights into the interactions among species across the reactive field when analyzing the counterflow configuration of complex fuel mixtures.

**Keywords:** nonpremixed flows; autoignition; heptane; ethanol

---

\*Corresponding author: kseshadri@ucsd.edu

## 1. Introduction

The laminar counterflow diffusion flame, as a steady state and one dimensional flame, is investigated to elucidate interaction between diffusion and chemistry[1]. This configuration has been widely studied to improve understanding of mechanism of inhibition effect and dilution limits[2][3][4].

Through the counterflow configuration, Seshadri [2] studied extinction of diffusion flame methanol, heptane and wood in the presence of suppressive agents such as nitrogen and water. Seiser et al. [3] elucidated the mechanisms of extinction and autoignition of n-heptane, finding that strain has greater influence on low-temperature chemistry than the temperature of the reactants. Ji et al. [4] investigated the impact of iso-butanol and ethanol on the auto-ignition of n-decane and n-heptane. It is observed that addition of iso-butanol and ethanol to n-decane or n-heptane elevated the auto-ignition temperature at low strain rates, indicating that iso-butanol and ethanol inhibits the low-temperature chemistry (LTC) of n-decane and n-heptane. These observations were further supported by sensitivity analysis.

Sensitivity analysis have been extensively employed to elucidate the influence of selected parameters on combustion. They are useful for identification and quantification of the role of selected parameters, reveal their predominant controlling influence alongside their indirect effect on changes in their values [5]. It is crucial in uncertainty analysis, estimation of parameter, and investigation or reduction of mechanism [6]. This approach is instrumental in understanding the sensitivity of the predicted outcomes or quantities of interest (QoIs) to uncertain parameters [7]. For example, sensitivity analysis facilitates quantification of the indirect influence of the rate constants of reactions in terms of temperature. However, the traditional sensitivity analysis in combustion research focuses on the systematic impact of parameters on output variables. It falls short of detailed explaining the direct influence between reactions and the output variables, nor the subsequent effects of these output variables changes on other output variables.

Another widely used method, path flux analysis (PFA) method, plays a crucial role in dissecting the production and consumption fluxes (pathways) in chemical mechanism. It is employed alongside in direct relation graph (DRG) method to identify critical species and reactions. Sun et al. demonstrated that the skeletal mechanisms refined by PFA exhibits enhanced accuracy compared to those derived by DRG method with the similar size in several cases[8] [9]. Path flux analysis could explicitly offer insight into the consumption and production of species in zero-dimensional models or single point in one-dimensional flame configura-

tion, facilitating analysis of kinetic mechanism. However, for the counterflow flame configuration, it has difficulty in elucidating the interaction cross different spatial points.

Recently, there have been numerous studies applying deep learning to chemical ordinary differential equations (ODEs). Ji et al.[10] developed the stiff-PINN approach that utilizes QSSA to enable the PINN to solve stiff chemical kinetics. The multiscale physics-informed neural network (MPINN) approach proposed by Weng et al.[11] is based on the regular physics-informed neural network (PINN) for solving stiff chemical kinetic problems with governing equations of stiff ODEs. Su et al.[12] employed a neural ordinary differential equation (Neural ODE) framework to optimize the kinetic parameters of reaction mechanisms, showing that the proposed algorithm can optimize stiff chemical models with sufficient accuracy, efficiency, and robustness. The forward propagation in neural networks shows a kind of equivalence to chemical ODEs. Thus, it is also possible to introduce sensitivity analysis methods for neural networks to chemical systems.

Zurada's sensitivity method, widely used in the analysis of neural networks for the reduction of training set size[13], employs the calculation of partial derivatives with respect to variables to elucidate their interdependencies. Inspired by Zurada's method and considering the unique characteristics of combustion chemistry alongside the governing equations of the counterflow configuration, we introduce a supplemental method. This method, grounded in the use of partial derivatives, aims to analyze the interplay across different temperature zones in counterflow flames. It is employed to provide a detailed explanation of the interactions between n-heptane and ethanol in their binary mixtures in counterflow diffusion flames.

## 2. Methodology

### 2.1. Analysis of reaction rate change

Similar to the approach taken in sensitivity analysis, the calculation of partial derivatives of the reaction rate with respect to the rate constant and species concentration serves as an important tool in reaction-rate-change-analysis. This method of analysis is designed to identify factors, either rate constant or species concentration, that primarily produce variations of rate of the  $n^{th}$  reaction  $\Delta\dot{\omega}$  under different conditions.

The rates of forward reaction  $\dot{\omega}_{f,k}$  and reverse reaction  $\dot{\omega}_{b,k}$  are determined by the product of the concentration of reactants or products  $c_i$  and their respective

rate constants  $k_{f,k}, k_{b,k}$ , expressed as follows:

$$\dot{\omega}_{f,k} = k_{f,k} \prod_{i=1}^n c_i^{\nu'_i}, \dot{\omega}_{b,k} = k_{b,k} \prod_{i=1}^n c_i^{\nu''_i} \quad (1)$$

The parameters  $\nu'_i, \nu''_i$  represent the stoichiometric coefficients for species  $i$  appearing as a reactant and as a product, respectively. Here, forward and reverse elemental reactions are treated as distinct entities. It is encapsulated by the equation:

$$\dot{\omega}_n = \begin{cases} \dot{\omega}_{f,k}, \text{ for forward reaction} \\ -\dot{\omega}_{b,k}, \text{ for reverse reaction} \end{cases} \quad \text{where } k = 1, 2, \dots, M \quad (2)$$

Here,  $M$  denotes the total number of elementary reactions before their separation into forward and reverse components, while  $n$  represents the  $n^{th}$  reactions after separation. The total number of reactions after separation,  $N$ , should be equal to  $2 \times M$  if all reactions include both forward and backward directions in the mechanism.

Change of reaction rate distributed to the  $n^{th}$  reaction rate constant change  $\Delta k_n$  and species  $i$  concentration change  $\Delta c_i$  are given as follows:

$$\Delta \dot{\omega}_n|_{k,n} = \Delta \dot{\omega}_n \times \frac{\partial \dot{\omega}_n / \partial k_n \times \Delta k_n}{\Delta \dot{\omega}_n^{\text{approx}}} \quad (3)$$

$$\Delta \dot{\omega}_n|_{c_i} = \Delta \dot{\omega}_n \times \frac{\partial \dot{\omega}_n / \partial c_i \times \Delta c_i}{\Delta \dot{\omega}_n^{\text{approx}}} \quad (4)$$

where the derivatives  $\Delta \dot{\omega}_n^{\text{approx}}, \partial \dot{\omega}_n / \partial k_n$  and  $\partial \dot{\omega}_n / \partial c_i$  are given by:

$$\Delta \dot{\omega}_n^{\text{approx}} = \frac{\partial \dot{\omega}_n}{\partial k_n} \times \Delta k_n + \sum_{i=1}^m \left( \frac{\partial \dot{\omega}_n}{\partial c_i} \times \Delta c_i \right) \quad (5)$$

$$\frac{\partial \dot{\omega}_n}{\partial k_n} = \prod_{i=1}^m c_i^{|\nu_i|}, \frac{\partial \dot{\omega}_n}{\partial c_i} = k_n \nu_i c_i^{|\nu_i|-1} \prod_{\substack{j=1 \\ i \neq j}}^m c_j^{|\nu_j|} \quad (6)$$

with

$$\nu_i = \nu''_i - \nu'_i$$

Here,  $m$  represents the total number of species involved in the  $n^{th}$  reaction. The term  $\Delta \dot{\omega}_n^{\text{approx}}$  is an approximation of  $\Delta \dot{\omega}_n$ , derived from the Taylor expansion

truncated at the first-order derivative. For an augmentation in precision, particularly concerning the reaction rate,  $\dot{\omega}_n$ , which manifests as a multivariate function, employing the second-order Taylor expansion provides deeper understanding. Details of corresponding derivation are provided in Appendix B.1.

## 2.2. Analysis of heat release rate change

Heat-release-rate-analysis aims to quantify the impact of changes in each species on overall heat release rate under different conditions. Heat release rate, denoted by  $\dot{Q}$ , is determined by summing the production of reaction enthalpy and net reaction rate for all relevant reactions. The relationship is mathematically represented as:

$$\dot{Q} = - \sum_k \Delta H_k \times \dot{\omega}_k \quad (7)$$

where  $\Delta H_k$  signifies the enthalpy change of the  $k^{th}$  reaction and  $\dot{\omega}_k$  represents the net rate of the  $k^{th}$  reaction. The net reaction rate further delineated as the difference between forward and backward reaction rates:

$$\dot{\omega}_k = \dot{\omega}_{f,k} - \dot{\omega}_{b,k} \quad (8)$$

The expression of heat release rate can be reformulated as follows:

$$\begin{aligned} \dot{Q} &= - \sum_k \Delta H_k \times (\dot{\omega}_{f,k} - \dot{\omega}_{b,k}) \\ &= - \sum_n \Delta H_n \times \dot{\omega}_n \end{aligned} \quad (9)$$

Heat-release-rate-analysis presented in this study primarily focuses on high-temperature zone where oxidizer temperature maintained constantly. Therefore, the local temperature at selected points for various mixtures are nearly identical, allowing for the reasonable assumption that reaction enthalpy  $\Delta H_n$ , which dependent on local temperature, remains constant. Therefore, the distribution of change of heat release rate,  $\Delta \dot{Q}$ , in response to changes in reaction rate constant,  $\Delta k_n$  and species concentrations  $\Delta c_i$ , are defined as follows:

$$\Delta \dot{Q}|_{k,n} = -\Delta H_n \times \Delta \dot{\omega}_n|_{k,n} \quad (10)$$

$$\Delta \dot{Q}|_{c_i} = \sum_n (-\Delta H_n \times \Delta \dot{\omega}_n|_{c_i}) \quad (11)$$

The terms  $\Delta\dot{Q}|_{k,n}$ ,  $\Delta\dot{Q}|_{c_i}$  represent the change of heat release rate attributed to the change of  $n^{th}$  reaction rate constant  $\Delta k_n$  and the change of species  $i$  concentration  $\Delta c_i$

### 2.3. Analysis of species concentration change

Analysis of species concentration change aims to quantifying the impact of reactions on changes of species and elucidate the interrelation among various species, particularly those achieving steady-state. While for species that do not satisfy steady-state approximation, the analysis incorporates the effects of species diffusion and convection. Furthermore, diagrams illustrating species equation terms provides a visual representation that enhances understanding interactions associated with these species.

For the counterflow flame, in steady state solution, governing equation for species  $i$  is given by :

$$0 = -\rho u \frac{dY_i}{dz} - \frac{dj_i}{dz} + W_i(\dot{\omega}_i^+ - \dot{\omega}_i^-) \quad (12)$$

$$\begin{aligned} \left[ -\rho u \frac{dY_i}{dz} \right] &: \text{convection term of species } i \\ \left[ -\frac{dj_i}{dz} \right] &: \text{diffusion term of species } i \\ \left[ W_i(\dot{\omega}_i^+ - \dot{\omega}_i^-) \right] &: \text{net production term of species } i \end{aligned}$$

Here,  $W_i$  denotes the molecular weight of species  $i$ .

Governing equation of species  $i$ , Eq.(12), could be rewritten as :

$$\dot{\omega}_i^- = -\rho u \frac{dY_i}{dz}/W_i - \frac{dj_i}{dz}/W_i + \dot{\omega}_i^+ \quad (13)$$

From Eq (13) , we could obtain a detailed expression for  $c_i$  as:

$$c_i = \frac{-\rho u \frac{dY_i}{dz}/W_i - \frac{dj_i}{dz}/W_i + \sum_{k=1}^r |\nu_{i,k}| [(1 - \delta'_{i,k})\dot{\omega}_{f,k} + \delta'_{i,k}\dot{\omega}_{b,k}]}{\sum_{k=1}^r |\nu_{i,k}| [\delta'_{i,k}w_{f,k}^{den} + (1 - \delta'_{i,k})w_{b,k}^{den}]} \quad (14)$$

Here, the terms  $[-\rho u \frac{dY_i}{dz} / W_i]$  and  $[-\frac{d j_i}{dz} / W_i]$  correspond to convective and diffusive mass transfer related term of species  $i$ , respectively. The detailed derivation from Eq (13) to Eq (14) is provided in Appendix B.2.

With the framework established by Eq (14), we can delve into analyzing changes in the concentration of species  $i$ . For the  $k^{th}$  elemental reaction, the contribution of its forward reaction rate with respect to species  $c_i$  is delineated as follows:

$$\Delta c_i|_{f,k} = \begin{cases} \frac{1}{\text{sum}} \times \frac{\partial c_i}{\partial w_{f,k}} \times \Delta w_{f,k}, \nu_{i,k} > 0 \\ \frac{1}{\text{sum}} \times \frac{\partial c_i}{\partial w_{f,k}^{\text{den}}} \times \Delta w_{f,k}^{\text{den}}, \nu_{i,k} < 0 \end{cases} \quad (15)$$

Similarly, its backward reaction rate contribution with respect to  $c_i$  is expressed as:

$$\Delta c_i|_{b,k} = \begin{cases} \frac{1}{\text{sum}} \times \frac{\partial c_i}{\partial w_{b,k}} \times \Delta w_{b,k}, \nu_{i,k} < 0 \\ \frac{1}{\text{sum}} \times \frac{\partial c_i}{\partial w_{b,k}^{\text{den}}} \times \Delta w_{b,k}^{\text{den}}, \nu_{i,k} > 0 \end{cases} \quad (16)$$

The contributions of convective mass transfer with respect to changes in  $c_i$  are identified as:

$$\Delta c_i|_{\text{convection}} = \frac{1}{\text{sum}} \times \frac{\partial c_i}{\partial (\rho u \frac{dY_i}{dz})} \times \Delta (\rho u \frac{dY_i}{dz}) \quad (17)$$

Similarly, the contributions of diffusion mass transfer with respect to changes in  $c_i$  is expressed as:

$$\Delta c_i|_{\text{diffusion}} = \frac{1}{\text{sum}} \times \frac{\partial c_i}{\partial (\frac{d j_i}{dz})} \times \Delta (\frac{d j_i}{dz}) \quad (18)$$

Here, sum defined as the aggregate of all contributions to changes in  $c_i$ , encapsulating those from both the forward and backward reaction rates, as well as

from the convective and diffusive mass transfers:

$$\begin{aligned} \text{sum} = & \sum \frac{\partial c_i}{\partial w_{f,k}} \times \Delta w_{f,k} + \sum \frac{\partial c_i}{\partial w_{f,k}^{den}} \times \Delta w_{f,k}^{den} \\ & + \sum \frac{\partial c_i}{\partial w_{f,k}^{den}} \times \Delta w_{f,k}^{den} + \sum \frac{\partial c_i}{\partial w_{b,k}^{den}} \times \Delta w_{b,k}^{den} \\ & + \frac{\partial c_i}{\partial (\rho u \frac{dY_i}{dz})} \times \Delta (\rho u \frac{dY_i}{dz}) + \frac{\partial c_i}{\partial (\frac{dj_i}{dz})} \times \Delta (\frac{dj_i}{dz}) \end{aligned} \quad (19)$$

Under the assumption that species  $i$  adheres to the steady-state approximation in the counterflow flame, governing equation terms exhibit the following relationship:

$$\left| \rho u \frac{dY_i}{dz} \right| \approx \left| \frac{dj_i}{dz} \right| \approx |W_i \dot{\omega}_i| \ll |W_i \dot{\omega}_i^+| \approx |W_i \dot{\omega}_i^-| \quad (20)$$

This suggests the magnitude of the convective and diffusive terms is considerably less than that of the production and consumption rates of species  $i$ . Consequently, upon disregarding the diffusion and convection terms, the concentration of species  $i$ , as depicted in Eq (14), simplifies to:

$$c_i = \frac{\sum_{k=1}^r |\nu_{i,k}| [(1 - \delta'_{i,k}) w_{f,k} + \delta'_{i,k} w_{b,k}]}{\sum_{k=1}^r |\nu_{i,k}| [\delta'_{i,k} w_{f,k}^{den} + (1 - \delta'_{i,k}) w_{b,k}^{den}]} \quad (21)$$

In this approximation, the contributions of both convection ( $\Delta c_i|_{\text{convection}}$ ) and diffusion ( $\Delta c_i|_{\text{diffusion}}$ ) are considered negligible. Furthermore, the term sum simplifies in the steady-state(ss) approximation as follows:

$$\begin{aligned} \text{sum}_{ss} = & \sum \frac{\partial c_i}{\partial w_{f,k}} \times \Delta w_{f,k} + \sum \frac{\partial c_i}{\partial w_{f,k}^{den}} \times \Delta w_{f,k}^{den} \\ & + \sum \frac{\partial c_i}{\partial w_{f,k}^{den}} \times \Delta w_{f,k}^{den} + \sum \frac{\partial c_i}{\partial w_{b,k}^{den}} \times \Delta w_{b,k}^{den} \end{aligned} \quad (22)$$

In scenarios where steady-state approximation is not applicable to species  $c_i$ , it becomes critical to consider all terms in governing equation, including those related to diffusion and convection. This comprehensive approach acknowledges

the comparable significance of diffusion and convection related terms alongside the chemical reaction term:

$$|\rho u \frac{dY_i}{dz}| \approx \left| \frac{dj_i}{dz} \right| \approx |W_i \dot{\omega}_i| \approx \max(W_i \dot{\omega}_i^+, W_i \dot{\omega}_i^-) \quad (23)$$

For the species not in steady state, visualizations delineating equation terms including convection, diffusion and net production terms, across the reactive field could help identify the origin of species undergoing diffusion or convection to other regions.

At a specific location, the dominance of one term over others in species equation highlights its pivotal role in shaping concentration profile. A positive value indicates an enhancement in concentration, whereas a negative value signifies a diminishing effect on concentration profile. This approach is elaborated in results and discussion section.

### 3. Demonstration of methodology

In hydrocarbons, such as n-alkanes, alkenes and cycloalkanes, low-temperature chemistry (LTC) is an intrinsic feature[14]. The LTC of n-heptane, for example, has been extensively investigated in various experimental setups, including the counterflow flame [3], shock tube[15], jet-stirred reactor[16], microgravity droplet flame [17]. Further studies have explored the impact of alcohol addition to n-heptane or other hydrocarbons in combustion characteristics[18]-[19]. While, traditional sensitivity method enhances the understanding of interactions within mechanisms, it falls short of detailing the influence between reactions and species cross the reactive field.

Thus, we demonstrated the analysis method proposed in this paper to explain interaction between ethanol and n-heptane in counterflow flame. Computation results are from this paper[], including species distribution, flame structure and critical conditions of auto-ignition, from the liquid fuel counterflow configuration. This computations are performed using Cantera [20] C++ interface with modified boundary conditions for liquid-gas interface of the liquid-pool. The mix-average transport model is applied to obtained steady-state solutions. Kinetic modeling is carried out using the San Diego Mechanism [21].

The fuels tested in this study include n-heptane, ethanol, and their mixtures with volumetric composition of 20% n-heptane + 80% ethanol, 30% n-heptane + 70% ethanol, 50% n-heptane + 50% ethanol, 80% n-heptane + 20% ethanol, and 90% n-heptane + 10% ethanol. The oxidizer used is air.

### 3.1. Auto-ignition temperature and heat release rate analysis

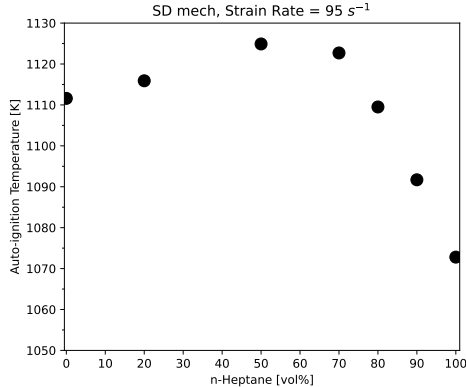


Figure 1: Auto-ignition temperature at low strain rate

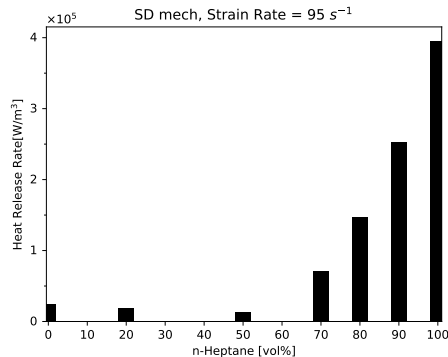


Figure 2: Heat release rate in the high-temperature zone [ $T_{ox}=1060$  K]

Fig. 1 illustrates auto-ignition temperature calculated at low strain rate,  $95\text{s}^{-1}$  for various volume fraction of ethanol in n-heptane. Additionally, Fig. 2 illustrates the variations in heat release rate, prior to auto-ignition, for these mixtures within the high-temperature zone, particularly focusing at 4.3mm from the fuel stream inlet, which corresponds to an oxidizer temperature,  $T_{ox}$ , of 1060K. A comparison between Fig. 1 and Fig. 2 indicates a direct correlation between the magnitude of heat release rate in this zone and the requisite temperature of auto-ignition ( $T_{ig}$ ). Among these examined mixtures, the 50%n-heptane-50%ethanol blend

stands out, necessitating the highest  $T_{ig}$ , a phenomenon that can be attributed to its significant lowest peak in heat release rate.

Fig. 2 illustrates that reducing the volume fraction of heptane from 100% to 90% leads to a significant decrease in heat release rate. Further heat-release-rate-analysis, as depicted in Fig. 3, attributes this decline of heat release rate predominantly and directly to changes of concentrations of HCO, HO<sub>2</sub>, OH, C<sub>2</sub>H<sub>5</sub>, C<sub>2</sub>H<sub>3</sub>, CH<sub>2</sub>O.

In contrast, the reduction in volume fraction of n-heptane from 50% to 20% is correlated to observable increase in heat release rate, as illustrated in Fig. 2. Similar heat-release-rate-analysis conducted and shown in Fig. 4, which indicated the increase of heat release rate is attributed to involvement of species such as CH<sub>3</sub>, HO<sub>2</sub>, OH, HCO, C<sub>2</sub>H<sub>5</sub>OH, CH<sub>3</sub>CHOH, CH<sub>2</sub>O.

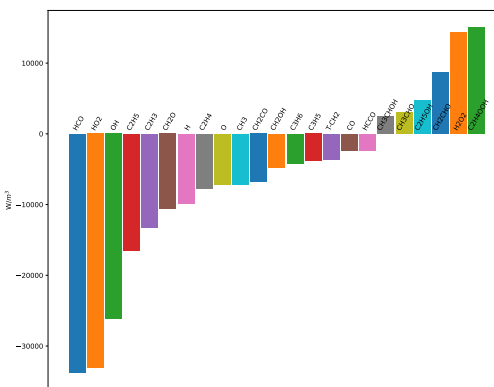


Figure 3: Distribution of heat release rate change from 100%n-heptane to 90%n-heptane

### 3.2. key species in n-heptane-dominant mixtures

The species contributing to heat release rate change could be categorized into two groups based on satisfaction of the steady-state approximation at the selected location.

For species that not satisfied steady-state approximation, their concentrations are governed by a combination of the diffusion term, convection term and chemical reaction term in species equation. Specifically, in Fig. 5, for CH<sub>2</sub>O, the net production rate peak is observed around 1.2mm, located in low-temperature zone where the LTC is highly activated. Additionally, positive value of diffusion term between 2mm and 5mm elucidate the role of diffusion term in promoting the transport of the CH<sub>2</sub>O from the low-temperature zone to the high-temperature

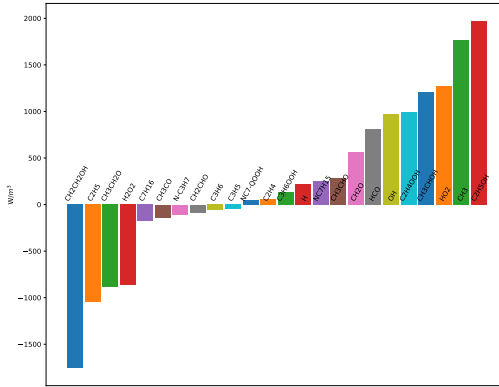


Figure 4: Heat release rate change from 50% n-heptane to 20% n-heptane

zone. Consequently, a decline of activity of LTC in the low-temperature region, caused by additional ethanol, leads to a reduction of diffusion effect, subsequently impacting heat release rate and auto-ignition at the high-temperature region. This effect is also evidenced by analysis of  $\text{CH}_2\text{O}$  concentration change, depicted in Fig. 6. The observed reduction of  $\text{CH}_2\text{O}$  in the high-temperature region is primarily attributed to decrement in diffusion term.

Similar patterns are observed with other radicals, such as hydroperoxyl ( $\text{H}_2\text{O}_2$ ), ethylene ( $\text{C}_2\text{H}_4$ ), and formaldehyde ( $\text{C}_2\text{H}_4$ ). The corresponding analyses and plots for these species are included in the supplemental materials, ranging from Fig. A.20 to Fig. A.23.

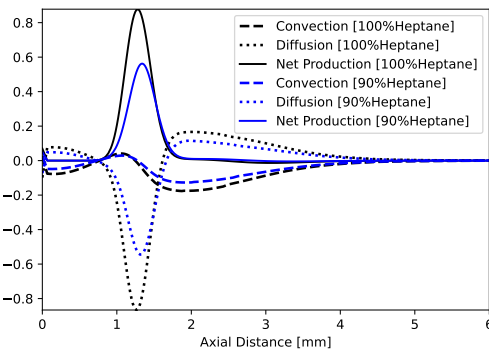


Figure 5:  $\text{CH}_2\text{O}$  Species equation terms

Within the context of steady-state species, their concentrations are predominantly governed by the the equilibrium between production and consumption rates

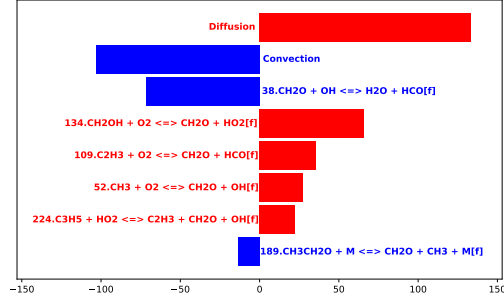


Figure 6: Contribution on  $\text{CH}_2\text{O}$  concentration change@4.2mm

at selected location. Among the species implicated in heat release rate reduction,  $\text{HCO}$ ,  $\text{HO}_2$ ,  $\text{OH}$ ,  $\text{C}_2\text{H}_5$  and  $\text{C}_2\text{H}_3$  are identified to be in the steady-state, indicating they produced at selected location concurrently consumed. The fluctuations in their concentrations were affected by specific reactions and variation of other species, elucidated through the analysis of concentration change.

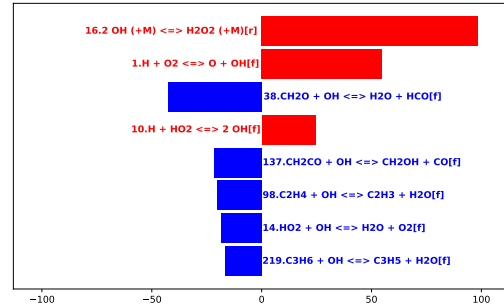


Figure 7: Contribution on OH concentration change@4.2mm

Fig. 7 demonstrates that concentration change of radical OH at the high-temperature zone primarily affected by reverse reaction of R16:2  $\text{OH} (+\text{M}) \rightleftharpoons \text{H}_2\text{O}_2 (+\text{M})$ , involving the decomposition of  $\text{H}_2\text{O}_2$ .  $\text{H}_2\text{O}_2$  is not in steady state and is diffused from the low-temperature zone.

Further concentration analysis reveals that concentration of  $\text{HO}_2$  is predominantly controlled by  $\text{HCO}$ , through R33:  $\text{HCO} + \text{O}_2 \Rightarrow \text{CO} + \text{HO}_2$ . Similarly,  $\text{HCO}$  concentration are primarily controlled by  $\text{CH}_2\text{O}$  and  $\text{OH}$  via R38:  $\text{CH}_2\text{O} + \text{OH} \Rightarrow \text{H}_2\text{O} + \text{HCO}$ . Concentration of  $\text{C}_2\text{H}_3$  is primarily regulated by  $\text{C}_2\text{H}_4$  by R98:  $\text{C}_2\text{H}_4 + \text{OH} \Rightarrow \text{C}_2\text{H}_3 + \text{H}_2\text{O}$ . Illustrative plots of these relationships are provided in the supplemental materials, as seen in Figures A.24, A.25, and A.26.

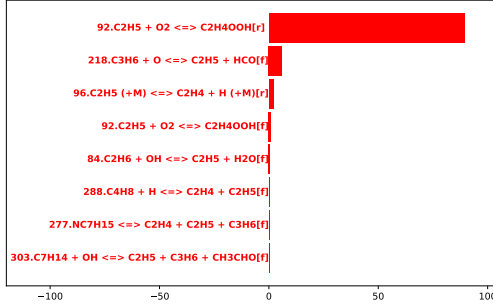


Figure 8: Contribution on  $\text{C}_2\text{H}_5$  concentration change@4.2mm

As mentioned before, both  $\text{CH}_2\text{O}$  and  $\text{C}_2\text{H}_4$  are mainly transported from the low-temperature region via diffusion.

Fig. 8 reveals that the radical  $\text{C}_2\text{H}_5$  is primarily influenced by R92:  $\text{C}_2\text{H}_5 + \text{O}_2 \rightleftharpoons \text{C}_2\text{H}_4\text{OOH}$ . However, it is actually a fast reaction so that the substantial consumption of  $\text{C}_2\text{H}_5$  in the forward reaction is counterbalanced by its production in the reverse reaction. Therefore, greater emphasis should be placed to the second reaction depicted in Fig. 8, R218:  $\text{C}_3\text{H}_6 + \text{O} \rightleftharpoons \text{C}_3\text{H}_6 + \text{HCO}$ , which is primarily affected by  $\text{C}_3\text{H}_6$ . Notably,  $\text{C}_3\text{H}_6$  is not in the steady state at the high-temperature zone and is primarily diffused from the low-temperature region.

In summary, radicals including  $\text{CH}_2\text{O}$ ,  $\text{C}_2\text{H}_4$ ,  $\text{C}_3\text{H}_6$  and  $\text{H}_2\text{O}_2$  predominantly diffused from the low-temperature zone, significantly influencing the heat release rate and auto-ignition process in the high-temperature zone.

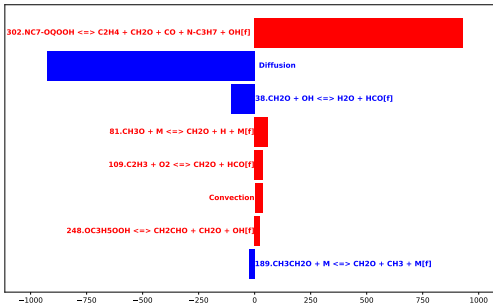


Figure 9: Contribution on  $\text{CH}_2\text{O}$  concentration change@1.1mm

This observation underscores the necessity of delineating the production mechanism of these species in the low-temperature zone. As indicated in Fig. 9 and Fig. 10,  $\text{CH}_2\text{O}$  and  $\text{C}_2\text{H}_4$  primarily produced through reaction R302:  $\text{NC}_7\text{OQOOH} \Rightarrow$

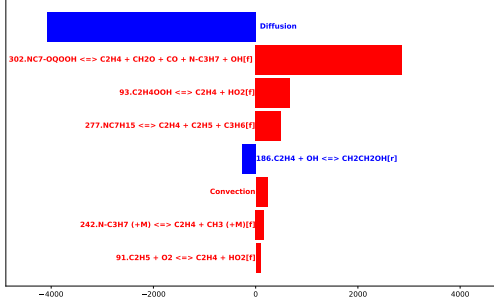
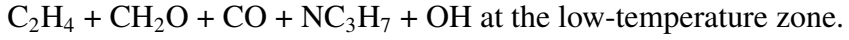


Figure 10: Contribution on  $C_2H_4$  concentration change@1.1mm



The origins of  $C_3H_6$  and  $H_2O_2$  in the low-temperature zone is notably complex. Fig. 11 proves that concentration of  $C_3H_6$  is predominantly regulated by  $NC_3H_7$ . Similarly, concentration analysis of  $H_2O_2$  and  $HO_2$  indicate  $H_2O_2$  is mainly converted from  $HO_2$ , which, in turn, is affected by  $NC_3H_7$ . These analysis results are further detailed in the supplemental materials, specifically in Figures A.27 and A.28.

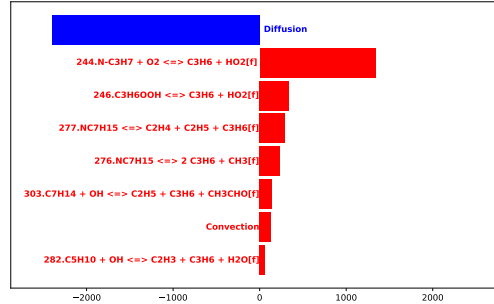


Figure 11: Contribution on  $C_3H_6$  concentration change@1.1mm

Given its pivotal role,  $NC_3H_7$  emerges as a crucial species impacting both  $H_2O_2$  and  $C_3H_6$ . It is primarily produced through reaction R302, as indicated in Fig. 12. Thus, in the low-temperature region, R302 exerts a direct influence on producing  $CH_2O$ ,  $C_2H_4$ , while indirectly affecting  $C_3H_6$  and  $HO_2$  via  $NC_3H_7$ .

Fig. 13 provides a comprehensive overview elucidating interplay between the low and high temperature zones in n-heptane-dominant mixtures. The addition of ethanol leads to competition of oxygen, resulting in a decreased of  $NC_7OQOOH$  concentration in the low-temperature zone. This reduction in concentration of

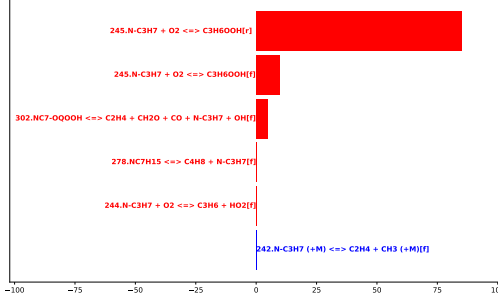


Figure 12: Contribution on  $\text{NC}_3\text{H}_7$  concentration change@1.1mm

$\text{NC}_7\text{OQOOH}$  subsequently diminishes the reaction rate of R302 and concentrations of its products. Ultimately, these effects propagated to the high-temperature zone through species diffusion.

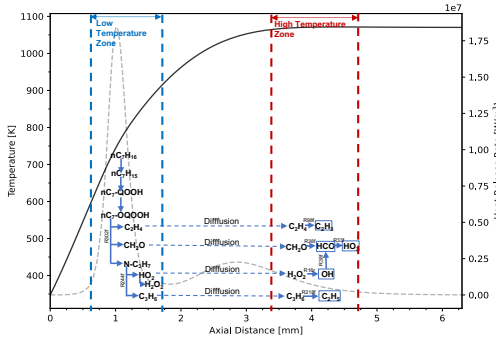


Figure 13: Heptane-dominant mixture overview. In the background, the black solid line represents the temperature profile and the grey dashed line indicates heat release rate

### 3.3. key species in ethanol-dominant mixtures

With the decrease of n-heptane's volume fraction from 50% to 20% and a concurrent increase in ethanol's volume fraction from 50% to 80%, it is observed the elevation in heat release rate in the high-temperature zone. This is primarily due to ethanol undergoing decomposition into three major products through hydrogen abstraction:  $\text{CH}_3\text{CHOH}$ ,  $\text{CH}_2\text{CH}_2\text{OH}$  and  $\text{CH}_3\text{CH}_2\text{O}$ .

The production of  $\text{CH}_3\text{CHOH}$ , mainly from reactions R172:  $\text{C}_2\text{H}_5\text{OH} + \text{OH} \Rightarrow \text{CH}_3\text{CHOH} + \text{H}_2\text{O}$  and R178:  $\text{C}_2\text{H}_5\text{OH} + \text{O} \Rightarrow \text{CH}_3\text{CHOH} + \text{OH}$ , plays a significant role in increasing heat release rate, as confirmed in Fig. 14. Notably,

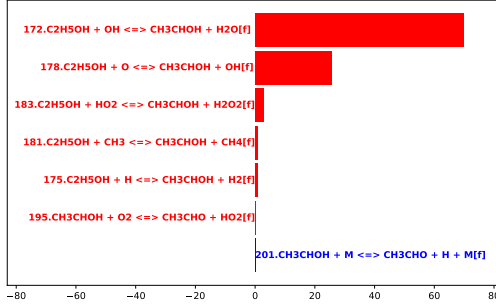


Figure 14: Contribution on  $\text{CH}_3\text{CHOH}$  concentration change@4.2mm

one pathway to form  $\text{CH}_3\text{CHOH}$ , via R183:  $\text{C}_2\text{H}_5\text{OH} + \text{H}_2\text{O}_2 \Rightarrow \text{CH}_3\text{CHOH} + \text{H}_2\text{O}_2$ , is accompanied by a significant production of  $\text{H}_2\text{O}_2$ , as depicted in Fig. 15b, with the peak production around 2.0mm-2.2mm, shown in Fig. 15a. It is subsequently diffused to the high-temperature region, contributing to the increase of OH concentration through the reverse reaction of R16:  $\text{H}_2\text{O}_2 (+\text{M}) \Rightarrow 2 \text{ OH} (+\text{M})$ , corroborated by Fig. 16. Additionally, the reverse reaction of R186, involving the decomposition of  $\text{CH}_2\text{CH}_2\text{OH}$ , contributes to the elevation of OH concentration, as indicated in Fig. 16.

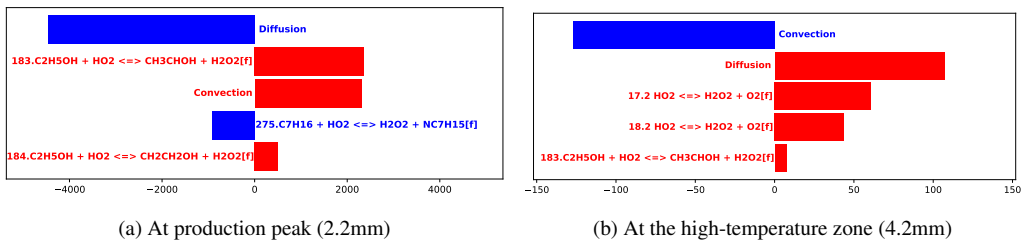


Figure 15: Contribution on  $\text{H}_2\text{O}_2$  concentration change

Furthermore, Fig. 17a demonstrates that the elevated levels of  $\text{CH}_3\text{CHOH}$  (through R195) and  $\text{CH}_3\text{CH}_2\text{O}$  (through R188) lead to an increase in  $\text{CH}_3\text{CHO}$ . And Fig. 17b further confirmed that part of increasing  $\text{CH}_3\text{CHO}$  diffused to the high-temperature region, thereby promoting heat release rate.

As illustrated in Fig. 18, the decomposition of  $\text{CH}_3\text{CH}_2\text{O}$  into  $\text{CH}_3$  and  $\text{CH}_2\text{O}$  through R189 :  $\text{CH}_3\text{CH}_2\text{O} (+\text{M}) \Rightarrow \text{CH}_3 + \text{CH}_2\text{O} (+\text{M})$ , with these products subsequently diffused to the high-temperature region. This process is augmented by R52:  $\text{CH}_3 + \text{O}_2 \Rightarrow \text{CH}_2\text{O} + \text{OH}$ , as illustrated in , wherein  $\text{CH}_3$  reacts with  $\text{O}_2$ , further elevating the concentration of  $\text{CH}_2\text{O}$ . The increase in  $\text{CH}_2\text{O}$  and  $\text{OH}$  leads

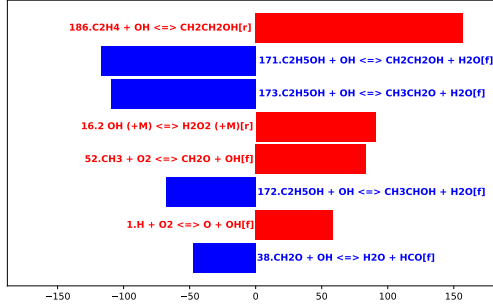


Figure 16: Contribution on OH concentration change @4.2mm

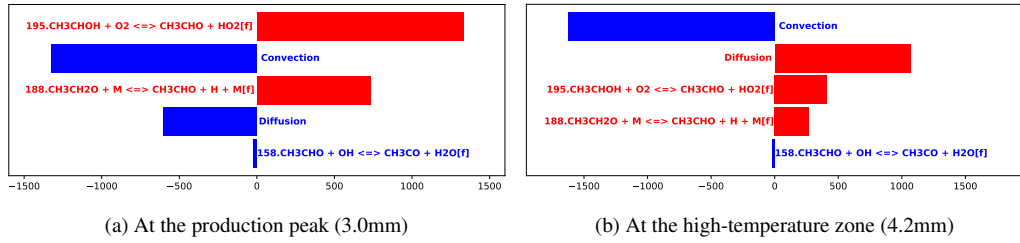


Figure 17: Contribution on  $\text{CH}_3\text{CHO}$  concentration change

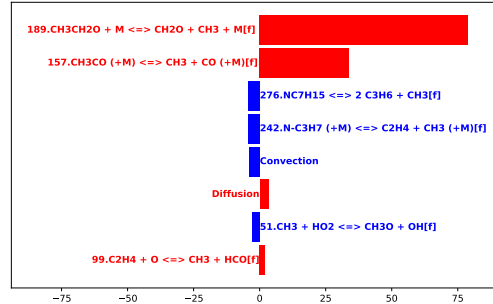


Figure 18: Contribution on  $\text{CH}_3$  concentration change@4.2mm

to a rise in  $\text{HCO}$ , increasing  $\text{HCO}$  contributes to enhanced concentration of  $\text{HO}_2$  in the high-temperature region. The concentration change analysis related to  $\text{CH}_2\text{O}$ ,  $\text{HCO}$  and  $\text{HO}_2$  are provided in Fig. A.29, Fig. A.30 and Fig. A.31 in supplemental materials.

The reaction pathway including  $\text{CH}_2\text{O}$ ,  $\text{HCO}$  and  $\text{HO}_2$  exhibits similarity in both n-heptane-dominant and ethanol-dominant mixtures. However, the concentration of  $\text{CH}_2\text{O}$  in n-heptane-dominant mixtures is predominantly influenced by

the low-temperature chemistry of n-heptane, whereas in ethanol-dominant mixtures,  $\text{CH}_2\text{O}$  is significantly affected, directly and indirectly, by  $\text{CH}_3\text{CH}_2\text{O}$ , through ethanol's hydrogen abstraction reaction, R189.

Additionally, the increase in  $\text{HO}_2$  partially results in heightened level of  $\text{H}_2\text{O}_2$  at the high-temperature region, as evidenced in Fig. 15b.

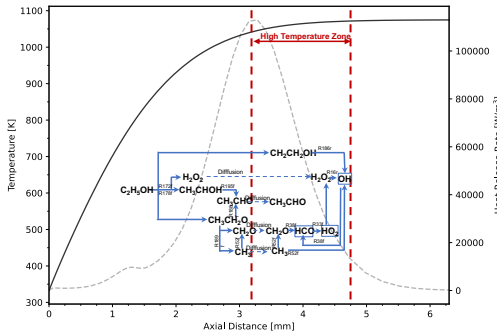


Figure 19: Ethanol-dominant mixture overview. In the background, the black solid line represents the temperature profile and the grey dashed line indicates heat release rate

Fig. 19 succinctly summarizes the reaction pathways and diffusive effects associated with ethanol-dominant mixtures. The observed increase in heat release rate, as ethanol volume fraction increased from 50% to 80%, is primarily attributable to species and reactions associated with ethanol's chemistry. In these mixtures, the influence of the inhibition of LTC is considered negligible.

### 3.4. Summary

The demonstrated example specifically targets n-heptane and ethanol dominant mixtures under the counterflow flame at low strain rate. Simulation results indicate a correlation between heat release rate and auto-ignition temperature. Further quantitative analyses, utilizing the proposed method, reveal that changes in the heat release rate in both n-heptane and ethanol dominant mixtures are directly associated with the alteration of several key species within the high-temperature zone.

In n-heptane-dominant mixtures, the investigation reveals that steady-state species at the high-temperature zone, including hydroxyl radicals (OH) and hydroperoxyl radicals (HO<sub>2</sub>), maintain the equilibrium between production and consumption rate, directly affecting heat release rate. Non-steady-state species at the high-temperature zone, such as CH<sub>2</sub>O and C<sub>2</sub>H<sub>4</sub> play significant roles in the auto-

ignition process, primarily due to their involvement in LTC at the low-temperature zone and subsequent diffusion to the high-temperature region.

For ethanol-dominant mixtures, the study highlights the observed increase in heat release rate with the increase in ethanol's volume fraction, attributing this elevation to the decomposition of ethanol into major products including  $\text{CH}_3\text{CHOH}$ ,  $\text{CH}_2\text{CH}_2\text{OH}$  and  $\text{CH}_3\text{CH}_2\text{O}$  radicals. The production of these species, particularly through hydrogen abstraction reactions is identified as the key pathway driving the observed increase in heat release rate.

The analysis result indicates the importance of species diffusion in the interaction between low and high temperature zones in n-heptane-dominant mixtures. Additionally, in the ethanol dominant mixtures, chemical kinetics are notably unaffected by n-heptane's LTC, highlighting the distinctive chemical pathways of ethanol and the influence of fuel composition on auto-ignition and heat release rate.

#### 4. Conclusion and outlook

This work proposed a method of analysis to reveal the relationship between change in heat release rate and variations of species, elucidating interaction among related species and the potential influence of species transport across different temperature zones in reactive field.

For demonstration, the study investigated the auto-ignition temperature of n-heptane and ethanol mixtures in a counterflow flame configuration under low strain rates. The analysis results indicate that this method effectively quantifies and compares the influence of chemical kinetics and species diffusion effects, detailing the complex interactions of critical species that influence the heat release rate.

Future research directions may include applying the method of analysis under varying strain rates and extending to other one-dimensional flame configurations. Additionally, given the complexity of preparing the overview for various mixtures, future efforts will focus on streamlining the analysis process through enhancing code automation.

## Appendix A. Concentration Analysis Results

### Appendix A.1. *n*-Heptane Dominant Mixtures

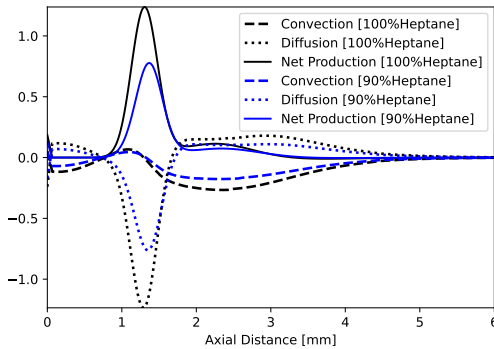


Figure A.20:  $\text{C}_2\text{H}_4$  Species equation terms

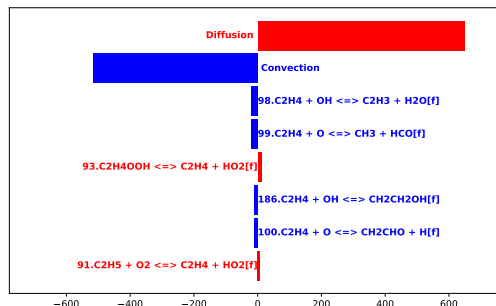


Figure A.21: Contribution on  $\text{C}_2\text{H}_4$  concentration change @4.2mm

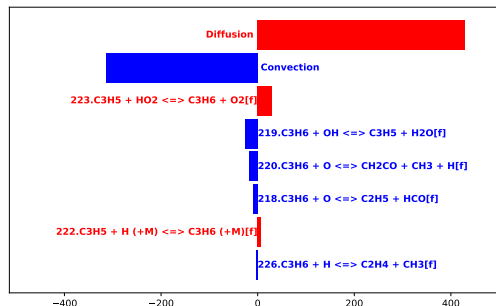


Figure A.22: Contribution on  $\text{C}_3\text{H}_6$  concentration change @4.2mm

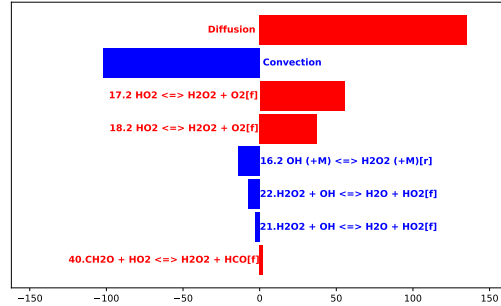


Figure A.23: Contribution on  $\text{H}_2\text{O}_2$  concentration change @4.2mm

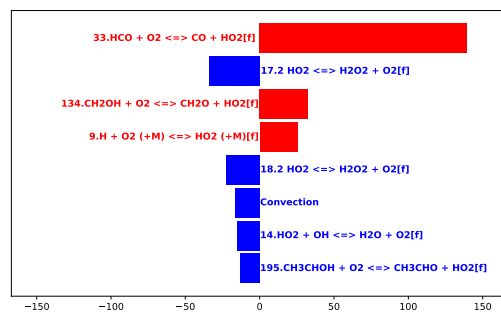


Figure A.24: Contribution on  $\text{HO}_2$  concentration change @4.2mm

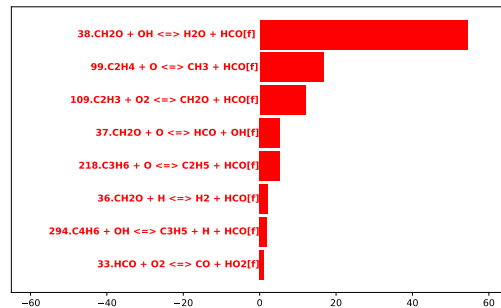


Figure A.25: Contribution on  $\text{HCO}$  concentration change @4.2mm

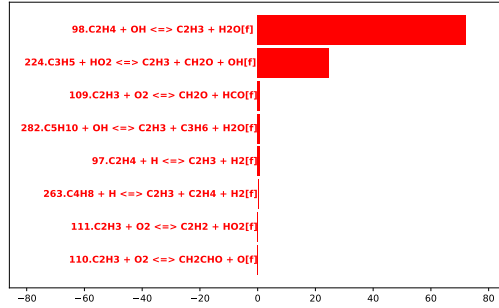


Figure A.26: Contribution on  $\text{C}_2\text{H}_3$  concentration change @4.2mm

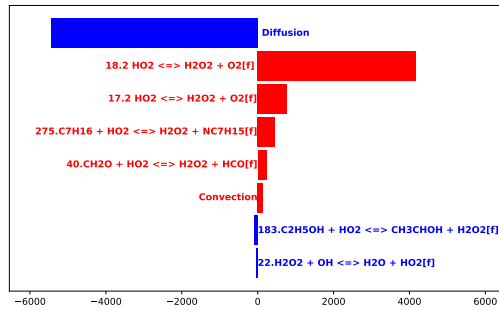


Figure A.27: Contribution on  $\text{H}_2\text{O}_2$  concentration change @1.1mm

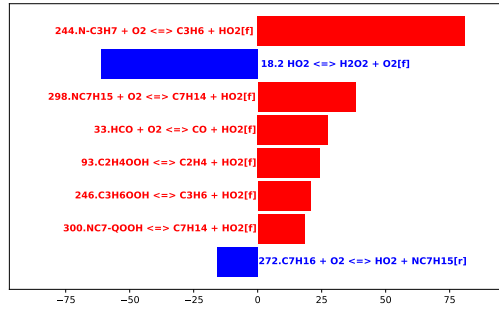


Figure A.28: Contribution on  $\text{HO}_2$  concentration change @1.1mm

## Appendix A.2. Ethanol Dominant Mixtures

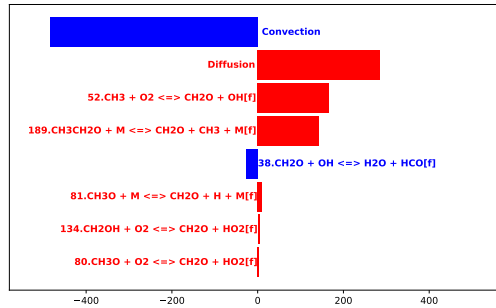


Figure A.29: Contribution on  $\text{CH}_2\text{O}$  concentration change @4.2mm

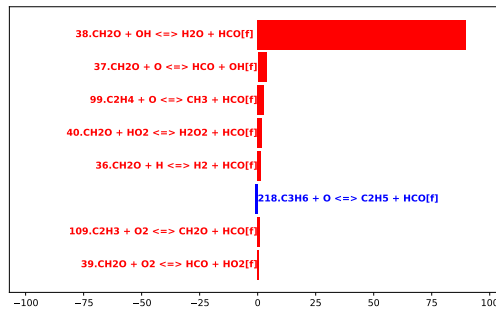


Figure A.30: Contribution on  $\text{HCO}$  concentration change @4.2mm

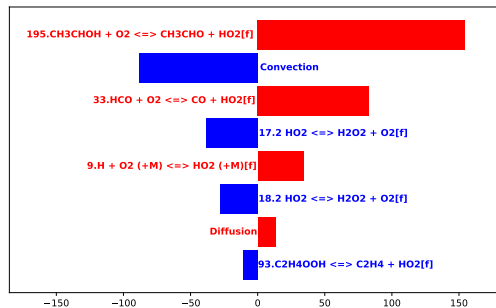


Figure A.31: Contribution on  $\text{HO}_2$  concentration change @4.2mm

## Appendix B. Details of Derivation of Analysis Method

### Appendix B.1. Derivation of reaction-rate-change-analysis

The formula below outlines the approximated reaction rate from the second-order Taylor expansion for function of multiple variables:

$$\Delta\dot{\omega}_n^{\text{approx}} = \sum_{i=0}^m \frac{\partial\dot{\omega}_n}{\partial x_i} \Delta x_i + \frac{1}{2} \sum_{i=0}^m \sum_{j=0}^m \frac{\partial^2\dot{\omega}_n}{\partial x_i \partial x_j} \Delta x_i \Delta x_j \quad (\text{B.1})$$

For simplification, let the variable  $x_i$  encompasses both the rate constant,  $k_n$ , and the species concentration,  $c_i$ , with  $x_0$  specifically denoting  $k_n$ .

$$x_i = \begin{cases} k_n, i = 0 \\ c_i, i \neq 0 \end{cases} \quad \text{where } i = 0, 1, \dots \quad (\text{B.2})$$

By employing the second derivative in Taylor series, the change in reaction rate attributed to  $\Delta x_i$  could be written as:

$$\Delta\dot{\omega}_n|_{x_i} = \frac{\partial\dot{\omega}_n}{\partial x_i} \Delta x_i + \frac{1}{2} \frac{\partial^2\dot{\omega}_n}{\partial x_i^2} (\Delta x_i)^2 + \sum_{\substack{j=0 \\ j \neq i}}^m \frac{1}{2} \frac{\partial^2\dot{\omega}_n}{\partial x_i \partial x_j} \Delta x_i \Delta x_j \quad (\text{B.3})$$

The term  $\frac{\partial\dot{\omega}_n}{\partial x_i} \Delta x_i + \frac{1}{2} \frac{\partial^2\dot{\omega}_n}{\partial x_i^2} (\Delta x_i)^2$  delineates the direct contribution of  $\Delta x_i$  to  $\Delta\dot{\omega}_n$ , encapsulating both linear and quadratic influences. While, the term  $\frac{1}{2} \frac{\partial^2\dot{\omega}_n}{\partial x_i \partial x_j} \Delta x_i \Delta x_j$  quantifies the synergistic influence on  $\Delta\dot{\omega}_n$  emanating from interaction between  $\Delta x_i$  and  $\Delta x_j$ . This synergistic influence could be symmetrically attributed to the influence from both  $\Delta x_i$  and  $\Delta x_j$ .

### Appendix B.2. Derivation of species concentration change

For the counterflow flame, in steady state solution, governing equation for species  $i$  is given by :

$$0 = -\rho u \frac{dY_i}{dz} - \frac{dj_i}{dz} + W_i(\dot{\omega}_i^+ - \dot{\omega}_i^-) \quad (\text{B.4})$$

Here,  $W_i$  denotes the molecular weight of species  $i$ . The production rate of species  $i$  is represented by  $\dot{\omega}_i^+$ , while  $\dot{\omega}_i^-$  symbolizes the consumption rate of species  $i$ . The production and consumption rate can be expressed as follows:

$$\begin{aligned}
\dot{\omega}_i^+ &= \sum_{k=1}^r \nu_{i,k} \left[ (1 - \delta'_{i,k}) \dot{\omega}_{f,k} - \delta'_{i,k} \dot{\omega}_{b,k} \right] \\
&= \sum_{k=1}^r |\nu_{i,k}| \left[ (1 - \delta'_{i,k}) \dot{\omega}_{f,k} + \delta'_{i,k} \dot{\omega}_{b,k} \right]
\end{aligned} \tag{B.5}$$

$$\begin{aligned}
\dot{\omega}_i^- &= \sum_{k=1}^r \nu_{i,k} \left[ -\delta'_{i,k} \dot{\omega}_{f,k} + (1 - \delta'_{i,k}) \dot{\omega}_{b,k} \right] \\
&= \sum_{k=1}^r |\nu_{i,k}| \left[ \delta'_{i,k} \dot{\omega}_{f,k} + (1 - \delta'_{i,k}) \dot{\omega}_{b,k} \right]
\end{aligned} \tag{B.6}$$

with  $\delta'_{i,k}$  defined as

$$\delta'_{i,k} = \begin{cases} 1 & \text{if } \nu_{i,k} < 0, \\ 0 & \text{if } \nu_{i,k} > 0 \end{cases} \tag{B.7}$$

The term

$$\nu_{i,k} = \nu''_{i,k} - \nu'_{i,k}$$

where  $\nu'_{i,k}$ ,  $\nu''_{i,k}$  are the stoichiometric coefficients for species  $i$  appearing as a reactant and as a product in  $k^{th}$  reaction, respectively.

Governing equation of species  $i$ , Eq.(12), could be rewritten as :

$$\dot{\omega}_i^- = -\rho u \frac{dY_i}{dz} / W_i - \frac{d\dot{j}_i}{dz} / W_i + \dot{\omega}_i^+ \tag{B.8}$$

While,  $\dot{\omega}_i^-$  can be expressed as:

$$\dot{\omega}_i^- = c_i \times \sum_{k=1}^r |\nu_{i,k}| \left[ \delta'_{i,k} w_{f,k}^{den} + (1 - \delta'_{i,k}) w_{b,k}^{den} \right] \tag{B.9}$$

where  $w_{f,k}^{den}$ ,  $w_{b,k}^{den}$  are defined as:

$$w_{f,k}^{den} = k_{f,k} \prod_{j=1}^n c_i^{\nu'_j - \delta_{i,j}}, \quad w_{b,k}^{den} = k_{b,k} \prod_{j=1}^n c_i^{\nu''_j - \delta_{i,j}} \tag{B.10}$$

and  $\delta_{i,j}$  indicates whether species  $j$  is species  $i$ :

$$\delta_{i,j} = \begin{cases} 1 & \text{if the species } j \text{ is species } i, \\ 0 & \text{otherwise.} \end{cases} \quad (\text{B.11})$$

Combining the Eq (13) and Eq (??), the concentration of substance  $i$ ,  $c_i$  can be derived from following expression:

$$c_i = \frac{-\rho u \frac{dY_i}{dz} / W_i - \frac{dj_i}{dz} / W_i + \dot{\omega}_i^+}{\sum_{k=1}^r |\nu_{i,k}| [\delta'_{i,k} w_{f,k}^{den} + (1 - \delta'_{i,k}) w_{b,k}^{den}]} \quad (\text{B.12})$$

Upon substituting Eq (??) into the equation above, we could obtain a detailed expression for  $c_i$  as:

$$c_i = \frac{-\rho u \frac{dY_i}{dz} / W_i - \frac{dj_i}{dz} / W_i + \sum_{k=1}^r |\nu_{i,k}| [(1 - \delta'_{i,k}) \dot{\omega}_{f,k} + \delta'_{i,k} \dot{\omega}_{b,k}]}{\sum_{k=1}^r |\nu_{i,k}| [\delta'_{i,k} w_{f,k}^{den} + (1 - \delta'_{i,k}) w_{b,k}^{den}]} \quad (\text{B.13})$$

Here, the terms  $[-\rho u \frac{dY_i}{dz} / W_i]$  and  $[-\frac{dj_i}{dz} / W_i]$  correspond to convective and diffusive mass transfer related term of species  $i$ , respectively.

## References

- [1] H. Tsuji, Counterflow diffusion flames, *Progress in Energy and Combustion Science* 8 (1982) 93–119. URL: <https://www.sciencedirect.com/science/article/pii/0360128582900156>. doi:doi:[https://doi.org/10.1016/0360-1285\(82\)90015-6](https://doi.org/10.1016/0360-1285(82)90015-6).
- [2] K. Seshadri, F. A. Williams, Laminar flow between parallel plates with injection of a reactant at high reynolds number, *International Journal of Heat and Mass Transfer* 21 (1978) 251–253. doi:doi:[https://doi.org/10.1016/0017-9310\(78\)90230-2](https://doi.org/10.1016/0017-9310(78)90230-2).
- [3] R. Seiser, H. Pitsch, K. Seshadri, W. Pitz, H. Gurran, Extinction and autoignition of n-heptane in counterflow configuration, *Proceedings of the Combustion Institute* 28 (2000) 2029–2037. doi:doi:[https://doi.org/10.1016/S0082-0784\(00\)80610-4](https://doi.org/10.1016/S0082-0784(00)80610-4).
- [4] L. Ji, A. Cuoci, A. Frassoldati, M. Mehl, T. Avedisian, K. Seshadri, Experimental and computational investigation of the influence of iso-butanol on autoignition of n-decane and n-heptane in non-premixed flows, *Proceedings of the Combustion Institute* 39 (2023) 2007–2015. doi:doi:<https://doi.org/10.1016/j.proci.2022.08.058>.
- [5] H. Rabitz, M. Kramer, D. Dacol, Sensitivity analysis in chemical kinetics, *Annual Review of Physical Chemistry* 34 (1983) 419–461. URL: <https://api.semanticscholar.org/CorpusID:97123635>.

[6] T. Turanyi, Applications of sensitivity analysis to combustion chemistry, *Reliability Engineering and System Safety* 57 (1997) 41–48. doi:doi:[https://doi.org/10.1016/S0951-8320\(97\)00016-1](https://doi.org/10.1016/S0951-8320(97)00016-1), the Role of Sensitivity Analysis in the Corroboration of Models and its Links to Model Structural and Parametric Uncertainty.

[7] T. A. O. Kalen Braman, V. Raman, Adjoint-based sensitivity analysis of flames, *Combustion Theory and Modelling* 19 (2015) 29–56. doi:doi:10.1080/13647830.2014.976274.

[8] W. Sun, Z. Chen, X. Gou, Y. Ju, A path flux analysis method for the reduction of detailed chemical kinetic mechanisms, *Combustion and Flame* 157 (2010) 1298–1307. doi:doi:<https://doi.org/10.1016/j.combustflame.2010.03.006>.

[9] W. Wang, X. Gou, An improved path flux analysis with multi generations method for mechanism reduction, *Combustion Theory and Modelling* 20 (2016) 203–220. doi:doi:10.1080/13647830.2015.1117660.

[10] W. Ji, W. Qiu, Z. Shi, S. Pan, S. Deng, Stiff-pinn: Physics-informed neural network for stiff chemical kinetics, *The Journal of Physical Chemistry A* 125 (2021) 8098–8106.

[11] Y. Weng, D. Zhou, Multiscale physics-informed neural networks for stiff chemical kinetics, *The Journal of Physical Chemistry A* 126 (2022) 8534–8543. URL: <https://doi.org/10.1021/acs.jpca.2c06513>. doi:doi:10.1021/acs.jpca.2c06513. arXiv:<https://doi.org/10.1021/acs.jpca.2c06513>, PMID: 36322833.

[12] X. Su, W. Ji, J. An, Z. Ren, S. Deng, C. K. Law, Kinetics parameter optimization of hydrocarbon fuels via neural ordinary differential equations, *Combustion and Flame* 251 (2023) 112732. URL: <https://www.sciencedirect.com/science/article/pii/S0010218023001177>. doi:doi:<https://doi.org/10.1016/j.combustflame.2023.112732>.

[13] J. M. Zurada, A. Malinowski, S. Usui, Perturbation method for deleting redundant inputs of perceptron networks, *Neurocomputing* 14 (1997) 177–193. doi:doi:[https://doi.org/10.1016/S0925-2312\(96\)00031-8](https://doi.org/10.1016/S0925-2312(96)00031-8).

[14] S. Liu, J. C. Hewson, J. H. Chen, H. Pitsch, Effects of strain rate on high-pressure non-premixed n-heptane autoignition in counterflow, *Combustion and Flame* 137 (2004) 320–339. doi:doi:<https://doi.org/10.1016/j.combustflame.2004.01.011>.

[15] J. Herzler, L. Jerig, P. Roth, Shock tube study of the ignition of lean n-heptane/air mixtures at intermediate temperatures and high pressures, *Proceedings of the Combustion Institute* 30 (2005) 1147–1153. doi:doi:<https://doi.org/10.1016/j.proci.2004.07.008>.

[16] C. Xie, M. Lailliau, G. Issayev, Q. Xu, W. Chen, P. Dagaut, A. Farooq, S. M. Sarathy, L. Wei, Z. Wang, Revisiting low temperature oxidation chemistry of n-heptane, *Combustion and Flame* 242 (2022) 112177. doi:doi:<https://doi.org/10.1016/j.combustflame.2022.112177>.

[17] T. I. Farouk, F. L. Dryer, Isolated n-heptane droplet combustion in microgravity: “cool flames” – two-stage combustion, *Combustion and Flame* 161 (2014) 565–581. doi:doi:<https://doi.org/10.1016/j.combustflame.2013.09.011>.

[18] J. Zhang, S. Niu, Y. Zhang, C. Tang, X. Jiang, E. Hu, Z. Huang, Experimental and modeling study of the auto-ignition of n-heptane/n-butanol mixtures, *Combustion and Flame* 160 (2013) 31–39. doi:doi:<https://doi.org/10.1016/j.combustflame.2012.09.006>.

[19] S. Guo, A. Cuoci, Y. Wang, C. T. Avedisian, L. Ji, K. Seshadri, N. DiReda, F. Alessio, Combustion Characteristics of a Tier II Gasoline Certification Fuel and its Surrogate with Iso-butanol: experiments and detailed numerical modeling, Technical Report, American Chemical Society, Chicago, Ill., 2022.

- [20] D. G. Goodwin, Moffat, H. K, S. Ingmar, Speth, R. L, Weber, B. W., Cantera: An object-oriented software toolkit for chemical kinetics, thermodynamics, and transport processes., 2023. doi:doi:10.5281/zenodo.8137090, version 3.0.0.
- [21] The San Diego Mechanism, <http://web.eng.ucsd.edu/mae/groups/combustion/mechanism.html>, 2016.